# An Airborne Laser Air Motion Sensing System. Part II: Design Criteria and Measurement Possibilities

LEIF KRISTENSEN

*Risø National Laboratory, Roskilde, Denmark*

DONALD H. LENSCHOW

*National Center for Atmospheric Research*, Boulder, CO 80307*

(Manuscript received 24 February 1986, in final form 21 July 1986)

ABSTRACT

A conically scanning Doppler lidar technique for measuring air motions from an aircraft is proposed in the companion paper (Keeler et al.). A theoretical analysis of this technique shows that, assuming isotropic turbulence, the technique is feasible for measuring air motions to scales small enough that the velocity spectra in a convective atmospheric boundary layer can be resolved well into the inertial subrange, and most of the turbulent motions that contribute to the vertical fluxes can be resolved. A scanning beam range of 10 m was selected to ensure that flow distortion induced by the aircraft will not significantly affect the velocity measurement. Thus, the technique offers improved accuracy over presently used immersion air motion sensors. An additional feature is the possibility of measuring mean vertical wind shear.

## 1. Introduction

The airborne laser air motion sensing system described in the companion paper by Keeler et al. (1986) has the potential to measure the three air velocity components from an aircraft more accurately than existing systems. One of the important questions that still needs to be addressed, however, is whether the conically scanning technique can provide sufficient spatial resolution to resolve the velocity fluctuations that contribute significantly to the vertical turbulent fluxes. We use, as a reasonable specification for aircraft boundary layer measurements, the capability to resolve at least 80% of the flux in a convective boundary layer at 35 m height, which is about the lowest level aircraft are likely to fly. Caughey and Kaimal (1977) present composite curves for heat flux cospectra at several heights in the boundary layer; cospectra for other scalars and the stress are similar. Their results show that this criteria can be met if wavelengths as short as ~100 m are resolved. This criteria applies only to an unstably stratified boundary layer. For a stably stratified boundary layer, shorter wavelengths than this are required to resolve the flux.

The main advantages of the conically scanning technique are its simplicity, its inherent absolute accuracy and its technical feasibility. Unfortunately, even if the laser could instantaneously measure the radial velocity at a point, as is assumed here, the velocity components are not obtained from measurements at one point, but on a helix. This paper presents a mathematical analysis of the conically scanning technique, discusses its limitations and applications to air velocity and vertical wind shear measurements from an aircraft, and presents criteria to be considered in designing the system.

## 2. Theoretical considerations

The conically scanning technique is implemented with a lidar mounted in the aircraft nose whose beam rotates through a conical scan with its axis along the aircraft heading and with an angle $\theta$ between the axis and the lidar beam. The rotation rate of the beam is $\omega_0$ (measured in rad $s^{-1}$). The Doppler velocity (measured along the beam) is measured at a mean distance $r$. The dimensions of the elongated averaging volume are assumed to be small enough compared to $r$ that the measured velocity can be considered a point measurement of the along-beam velocity component along a path that, as seen from the aircraft, is a circle with radius $r\sin\theta$. This is illustrated schematically in Fig. 2.

We use a Cartesian coordinate system that is fixed with respect to the aircraft. The $\mathbf{i}_1$ direction is along the longitudinal axis of the aircraft pointing towards the rear. The $\mathbf{i}_3$ unit vector is perpendicular to $\mathbf{i}_1$ in the vertical plane of the aircraft which contains $\mathbf{i}_1$. Finally, the lateral direction is defined by

$$\mathbf{i}_2 = \mathbf{i}_3 \times \mathbf{i}_1 . \quad (1)$$

* The National Center for Atmospheric Research is sponsored by the National Science Foundation.

In this coordinate system, the Doppler velocity is measured at time $t$ at the location

$$\mathbf{r}(t) = -r\cos\theta\mathbf{i}_1 + r\sin\theta\cos\omega_0 t\mathbf{i}_2 + r\sin\theta\sin\omega_0 t\mathbf{i}_3. \quad (2)$$

The velocity field $\mathbf{u}(\mathbf{r}, t)$ (in the same frame of reference) is a function of the three variables $\mathbf{r}$ and $t$,

$$\mathbf{u}(\mathbf{r}, t) = u_1(\mathbf{r}, t)\mathbf{i}_1 + u_2(\mathbf{r}, t)\mathbf{i}_2 + u_3(\mathbf{r}, t)\mathbf{i}_3. \quad (3)$$

The measured Doppler velocity then becomes

$$\begin{aligned} u_D(t) &= \mathbf{u}(\mathbf{r}(t), t)\cdot\mathbf{r}(t)/r \\ &= -u_1(\mathbf{r}(t), t)\cos\theta + u_2(\mathbf{r}(t), t)\sin\theta\cos\omega_0 t \\ &\quad + u_3(\mathbf{r}(t), t)\sin\theta\sin\omega_0 t. \end{aligned} \quad (4)$$

We assume here that the velocity field is homogeneous and stationary. The ensemble or long-term means of the components of $\mathbf{u}(\mathbf{r}, t)$ in the aircraft frame of reference are

$$\begin{aligned} \langle u_1(\mathbf{r}(t), t)\rangle &= UD^{-1} = -\frac{\omega_0}{2\pi\cos\theta}\left\langle\int_{t-2\pi/\omega_0}^{t} u_D(t')dt'\right\rangle \\ \langle u_2(\mathbf{r}(t), t)\rangle &= UD^{-1}\tan\beta \\ &= \frac{\omega_0}{\pi\sin\theta}\left\langle\int_{t-2\pi/\omega_0}^{t} u_D(t')\cos\omega_0 t'dt'\right\rangle \\ \langle u_3(\mathbf{r}(t), t)\rangle &= UD^{-1}\tan\alpha \\ &= \frac{\omega_0}{\pi\sin\theta}\left\langle\int_{t-2\pi/\omega_0}^{t} u_D(t')\sin\omega_0 t'dt'\right\rangle \end{aligned} \quad (5)$$

where $D = (1 + \tan^2\alpha + \tan^2\beta)^{1/2}$. The angles of attack $\alpha$ and sideslip $\beta$ are illustrated schematically in Fig. 1. Here $\alpha$ is the angle between the projection of $\mathbf{u}$ on the plane defined by $\mathbf{i}_1$ and $\mathbf{i}_3$, and $\mathbf{i}_1$, the conical scan axis, with $\alpha$ positive in the downward direction; $\beta$ is the angle between the projection of $\mathbf{u}$ on the plane defined by $\mathbf{i}_1$ and $\mathbf{i}_2$, and $\mathbf{i}_1$, with the clockwise (looking from above) rotation positive; $U$ is the mean true airspeed; and the brackets denote ensemble averaging. In conventional gust probe systems now in use, the flow angles $\alpha$ and $\beta$ are measured, and the air velocity components are calculated using the middle expressions of (5) (Lenschow, 1986), while the expressions on the right are used in the implementation of the conically scanning technique.

If we assume, for now, that $\mathbf{u}(\mathbf{r}(t), t)$ is constant for an entire revolution $2\pi/\omega_0$, we have

$$u_1 = -\frac{\omega_0}{2\pi\cos\theta}\int_{t-2\pi/\omega_0}^{t} u_D(t')dt', \quad (6)$$

$$u_2 = \frac{\omega_0}{\pi\sin\theta}\int_{t-2\pi/\omega_0}^{t} u_D(t')\cos\omega_0 t'dt', \quad (7)$$

$$u_3 = \frac{\omega_0}{\pi\sin\theta}\int_{t-2\pi/\omega_0}^{t} u_D(t')\sin\omega_0 t'dt'. \quad (8)$$

This condition is, in general, not fulfilled. Therefore, the question is how well $\mathbf{v}(t)$, which is defined by (6)–(8) without the assumption that $\mathbf{u}(\mathbf{r}(t),t)$ is constant from $t - 2\pi/\omega_0$ to $t$, represents the velocity $\mathbf{u}$ at the point $-r\cos\theta\cos\mathbf{i}_1$ and time $t$. From (5), we see that

$$\langle v_1(t)\rangle = UD^{-1}, \quad (9)$$

$$\langle v_2(t)\rangle = UD^{-1}\tan\beta, \quad (10)$$

$$\langle v_3(t)\rangle = UD^{-1}\tan\alpha. \quad (11)$$

We make one further assumption here for mathematical convenience. We assume that the mean air velocity vector relative to the aircraft $\mathbf{U}$ is aligned with the conical scan axis $\mathbf{i}_1$. This has a negligible effect on the conclusions that follow, since the values of $\alpha$ and $\beta$ are normally small. The geometry of the conically scanning technique is shown schematically in Fig. 2. Typically, $\alpha$ does not vary by more than a few degrees during a flight unless the aircraft is near stall or encounters severe turbulence. Variations in $\beta$ are typically even smaller, except possibly during turns. In turbulence, variations in $\alpha$ and $\beta$ can be estimated by the relations

$$\alpha' \approx v_3'/U,$$

$$\beta' \approx v_2'/U, \quad (12)$$

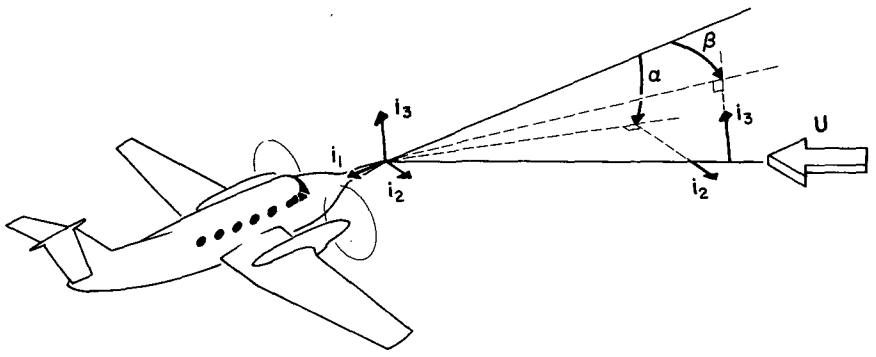


FIG. 1. Schematic illustration of the airflow incidence angles $\alpha$ and $\beta$.

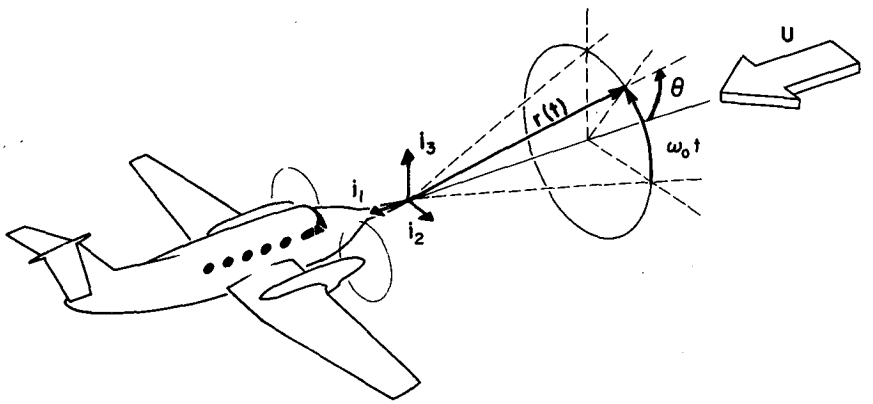


FIG. 2. Schematic illustration of the geometry of the airborne conically scanning lidar.

where the prime indicates departures from the means. With this assumption, (9)–(11) reduce to

$$\langle v_1(t)\rangle = \mathbf{U} = -\langle u_D(t)\rangle/\cos\theta,$$
$$\langle v_2(t)\rangle = \langle v_3(t)\rangle = 0. \tag{13}$$

Subtracting the means, we get for the fluctuating components of $\mathbf{v}(t)$

$$v_1'(t) = \frac{-\omega_0}{2\pi\cos\theta}\int_{t-2\pi/\omega_0}^{t} u_D'(t')dt', \tag{14}$$

$$v_2'(t) = \frac{\omega_0}{\pi\sin\theta}\int_{t-2\pi/\omega_0}^{t} u_D'(t')\cos\omega_0 t'dt', \tag{15}$$

$$v_3'(t) = \frac{\omega_0}{\pi\sin\theta}\int_{t-2\pi/\omega_0}^{t} u_D'(t')\sin\omega_0 t'dt', \tag{16}$$

where the primed velocity components indicate departures from the means.

We define our criteria of performance to be how well the power spectra of $\mathbf{v}(t)$ represent the power spectra of $\mathbf{u}(-r\cos\theta\mathbf{i}_1, t)$. That is, how close the transfer functions for the spectra of $\mathbf{u}$ and $\mathbf{v}$ are to unity over the entire spectral frequency domain. In order to calculate the power spectra of $\mathbf{v}(t)$, we must first determine the power spectrum of the measured Doppler velocity $u_D(t)$. (This should not be confused with the Doppler spectrum.) The most straightforward way to do this is to first determine the autocovariance function

$$R_D(t', t'') = \langle u_D'(t')u_D'(t'')\rangle. \tag{17}$$

Using (4) and assuming that $\mathbf{u}(\mathbf{r}, t)$ is homogeneous and stationary, we obtain

$$\begin{aligned} R_D(t', t'') &= R_{11}(\mathbf{r}(t'') - \mathbf{r}(t'), t'' - t')\cos^2\theta \\ &+ R_{22}(\mathbf{r}(t'') - \mathbf{r}(t'), t'' - t')\sin^2\theta\cos\omega_0 t'\cos\omega_0 t'' \\ &+ R_{33}(\mathbf{r}(t'') - \mathbf{r}(t'), t'' - t')\sin^2\theta\sin\omega_0 t'\sin\omega_0 t'' \\ &- \{R_{12}(\mathbf{r}(t'') - \mathbf{r}(t'), t'' - t')\cos\omega_0 t'' \\ &+ R_{21}(\mathbf{r}(t'') - \mathbf{r}(t'), t'' - t')\cos\omega_0 t'\}\cos\theta\sin\theta \\ &- \{R_{13}(\mathbf{r}(t'') - \mathbf{r}(t'), t'' - t')\sin\omega_0 t'' \\ &+ R_{31}(\mathbf{r}(t'') - \mathbf{r}(t'), t'' - t')\sin\omega_0 t'\}\cos\theta\sin\theta \\ &+ \{R_{23}(\mathbf{r}(t'') - \mathbf{r}(t'), t'' - t')\cos\omega_0 t'\sin\omega_0 t'' \\ &+ R_{32}(\mathbf{r}(t'') - \mathbf{r}(t'), t'' - t')\cos\omega_0 t''\sin\omega_0 t'\}\sin^2\theta, \end{aligned} \tag{18}$$

where

$$R_{ij}(\mathbf{r}'' - \mathbf{r}', t'' - t') = \langle u_i'(\mathbf{r}', t')u_j'(\mathbf{r}'', t'')\rangle \tag{19}$$

is the autocovariance tensor of $\mathbf{u}(\mathbf{r}, t)$.

In order to proceed further, we make the assumption of "frozen turbulence" (i.e., Taylor's hypothesis). This is a valid assumption for the case considered here, since the true airspeed $U$ is much larger than the velocity fluctuations. With this assumption,

$$R_{ij}(\mathbf{r}(t'') - \mathbf{r}(t'), t'' - t') = R_{ij}(\rho(t', t''), 0), \tag{20}$$

where

$$\rho(t', t'') = \mathbf{r}(t'') - \mathbf{r}(t') - U(t'' - t')\mathbf{i}_1. \tag{21}$$

Using (2), and introducing the unit vector

$$I(t) = -\mathbf{i}_2\sin\omega_0 t + \mathbf{i}_3\cos\omega_0 t, \tag{22}$$

(21) can be written as

$$\rho(t', t'') = -U(t'' - t')\mathbf{i}_1 + 2r\sin\theta\sin\left(\frac{\omega_0(t'' - t')}{2}\right)I\left(\frac{t' - t''}{2}\right). \tag{23}$$

The magnitude of $\rho(t', t'')$ is not a function of absolute time $(t' + t'')/2$. We see immediately that

$$\rho_2 = |\rho(t', t'')|^2 = U^2(t'' - t')^2 + 4r^2\sin^2\theta\sin^2\left(\frac{\omega_0(t'' - t')}{2}\right). \tag{24}$$

We now make the assumption that the turbulence is isotropic. This seems reasonable for the case considered here, since the magnitude of $r$ is about 10 m, while the scale of the turbulence is typically 100 m or more.

For isotropic turbulence, we have (Lumley and Panofsky, 1964)

$$R_{ij}(\rho,0)\equiv R_{ij}(\rho)=R_T(\rho)\delta_{ij}+(R_L(\rho)-R_T(\rho))\frac{\rho_i\rho_j}{\rho^2} \quad (25)$$

where the two scalar functions $R_L(\rho)$ and $R_T(\rho)$ of the scalar argument $\rho$ are the longitudinal and transversal autocovariance functions, respectively.

Substituting (25) into (18), and using (20)–(24), we find after some manipulation that $R_D(t', t'')$ depends only on $t'$ and $t''$ through the difference

$$\tau = t''-t'. \quad (26)$$

We get

$$R_D(\tau)\equiv R_D(0,t''-t')=R_L(\rho)\{\cos^2\theta+\sin^2\theta\cos\omega_0\tau\}+\sin^2\theta\{R_T(\rho)-R_L(\rho)\}\times\left\{\cos^2\frac{\omega_0\tau}{2}-[(U\tau)^2-4r^2\cos^2\theta]\sin^2\frac{\omega_0\tau}{2}\Big/\rho^2\right\} \quad (27)$$

with $\rho$ given by (24). The power spectrum of the Doppler velocity $u_D(t)$ is now given by

$$\phi_D(\omega)=\frac{1}{2\pi}\int_{-\infty}^{\infty}R_D(\tau)e^{-i\omega\tau}d\tau. \quad (28)$$

Next we derive the spectra for $\mathbf{v}'(t)$, given by (12)–(14). Since we have assumed isotropy, the spectra of $v_2'(t)$ and $v_3'(t)$ are equal. Therefore, we need only derive spectra for the longitudinal component $v_1'(t)$ and the transversal component $v_2'(t)$, denoted by $\phi_1(\omega)$ and $\phi_2(\omega)$, respectively, from the measured power spectrum of the Doppler velocity $\phi_D(\omega)$.

We proceed by emulating the scheme usually applied to experimental calculation of spectra of measured time series. We start by Fourier transforming the time series (13) and (14) over a finite record of duration $T$,

$$\hat{v}_i(T;\omega)=\frac{1}{2\pi}\int_{-T/2}^{T/2}v_i'(t)e^{i\omega t}dt, \quad i=1,2. \quad (29)$$

The spectrum $\phi_i(\omega)$ is defined by first calculating

$$\phi_i(T;\omega)=\frac{2\pi}{T}\langle\hat{v}_i(T;\omega)\hat{v}_i^*(T;\omega)\rangle, \quad i=1,2, \quad (30)$$

then letting $T$ go to infinity; viz,

$$\phi_i(\omega)=\lim_{T\to\infty}\phi_i(T;\omega), \quad i=1,2. \quad (31)$$

From (14) and (29), the longitudinal component can be written as

$$\hat{v}_1(T;\omega)=-\frac{1}{2\pi}\int_{-T/2}^{T/2}e^{i\omega t}dt\frac{\omega_0}{2\pi\cos\theta}\int_{t-2\pi/\omega_0}^{t}u_D'(s)ds. \quad (32)$$

Substitution into (30) yields

$$\phi_1(T;\omega)=\frac{1}{2\pi T}\int_{-T/2}^{T/2}e^{i\omega t'}dt'\int_{-T/2}^{T/2}e^{-i\omega t''}dt''\int_{t'-2\pi/\omega_0}^{t'}ds'\times\int_{t''-2\pi/\omega_0}^{t''}ds''R_D(s''-s')\frac{\omega_0^2}{4\pi^2\cos^2\theta}$$
$$=\frac{1}{2\pi T}\int_{-T/2}^{T/2}e^{i\omega t'}dt'\int_{-T/2}^{T/2}e^{-i\omega t''}dt''\int_{t'-2\pi/\omega_0}^{t'}ds'\times\int_{t''-2\pi/\omega_0}^{t''}ds''\int_{-\infty}^{\infty}\phi_D(\omega')e^{i\omega'(s''-s')}d\omega'\frac{\omega_0^2}{4\pi^2\cos^2\theta}, \quad (33)$$

where we have made use of the inverse Fourier transformation

$$R_D(\tau)=\int_{-\infty}^{\infty}\phi_D(\omega)e^{i\omega t}d\omega. \quad (34)$$

Carrying out the integrations in (33),

$$\phi_1(T;\omega)=\frac{1}{\cos^2\theta}\int_{-\infty}^{\infty}\frac{\sin^2\left(\pi\frac{\omega'}{\omega_0}\right)}{\left(\pi\frac{\omega'}{\omega_0}\right)^2}\frac{1}{2\pi T}\frac{\sin^2\left(\frac{\omega-\omega'}{2}T\right)}{\left(\frac{\omega-\omega'}{2}\right)^2}\phi_D(\omega')d\omega'. \quad (35)$$

In the limit of $T$ going to infinity we have

$$\lim_{T\to\infty}\frac{\sin^2\left(\frac{\omega T}{2}\right)}{T\left(\frac{\omega}{2}\right)^2}=2\pi\delta(\omega), \quad (36)$$

where $\delta(\omega)$ is Dirac's delta function. We see immediately that

$$\phi_1(\omega)=\lim_{T\to\infty}\phi_1(T;\omega)=\frac{1}{\cos^2\theta}\times\frac{\sin^2\left(\pi\frac{\omega}{\omega_0}\right)}{\left(\pi\frac{\omega}{\omega_0}\right)^2}\phi_D(\omega). \quad (37)$$

For the transverse velocity component, we have

$$\hat{v}_2(T;\omega)=\frac{1}{2\pi}\int_{-T/2}^{T/2}e^{i\omega t}dt\frac{\omega_0}{\phi\sin\theta}\int_{t-2\pi/\omega_0}^{t}u_D'(s)\cos\omega_0 s ds. \quad (38)$$

Consequently,

$$\phi_2(T;\omega)=\frac{1}{2\pi T}\int_{-T/2}^{T/2}e^{i\omega t'}dt'\int_{-T/2}^{T/2}e^{-i\omega t''}dt''\int_{t'-2\pi/\omega_0}^{t'}ds'\times\int_{t''-2\pi/\omega_0}^{t''}ds''R_D(s''-s')\times\cos\omega_0 s'\cos\omega_0 s''\frac{\omega_0^2}{\pi^2\sin^2\theta}$$

$$= \frac{1}{2\pi T}\int_{-T/2}^{T/2} e^{i\omega t'}dt' \int_{-T/2}^{T/2} e^{-i\omega t''}dt'' \int_{-\pi/\omega_0}^{\pi/\omega_0} ds' \int_{-\pi/\omega_0}^{\pi/\omega_0} ds''$$
$$\times R_D(s''-s'+t''-t') \times \cos[\omega_0(s'+t')]$$
$$\times \cos[\omega_0(s''+t'')] \frac{\omega_0^2}{\pi^2 \sin^2\theta}. \quad (39)$$

Substituting (34) into (39), we see that $\phi_2(T;\omega)$ can be written as

$$\phi_2(T;\omega) = \frac{1}{\sin^2\theta}\int_{-\infty}^{\infty} \frac{1}{2\pi T}|H(T;\omega_0,\omega,\omega')|^2 \phi_D(\omega')d\omega', \quad (40)$$

where

$$H(T;\omega_0,\omega,\omega') = \frac{\omega_0}{\pi}\int_{-T/2}^{T/2} dt \int_{-\pi/\omega_0}^{\pi/\omega_0} ds e^{i(\omega t-\omega'(s+t))} \cos[\omega_0(s+t)]. \quad (41)$$

Carrying out the integrations, $H$ becomes

$$H(T;\omega_0,\omega,\omega') = \frac{\sin\left(\pi\frac{\omega}{\omega_0}\right)}{\pi\frac{\omega}{\omega_0}} \times \left[\frac{\sin\left(\frac{\omega-\omega'+\omega_0}{2}T\right)}{\frac{\omega-\omega'+\omega_0}{2}} + \frac{\sin\left(\frac{\omega-\omega'-\omega_0}{2}T\right)}{\frac{\omega-\omega'-\omega_0}{2}}\right] \quad (42)$$

which, for increasing values of large $T$, approaches

$$\lim_{T\to\infty} H(T;\omega_0,\omega,\omega') = 2\pi \frac{\sin\left(\pi\frac{\omega}{\omega_0}\right)}{\pi\frac{\omega}{\omega_0}} [\delta(\omega-\omega'+\omega_0)+\delta(\omega-\omega'-\omega_0)]. \quad (43)$$

Multiplying the right-hand sides of (42) and (43) together results in the following expression for $|H|^2$ in the limit of large $T$:

$$|H(T;\omega_0,\omega,\omega')|^2 = 2\pi T \frac{\sin^2\left(\pi\frac{\omega}{\omega_0}\right)}{\left(\pi\frac{\omega}{\omega_0}\right)^2}\left[1+\pi\frac{\delta(\omega_0)}{T}\right] \times [\delta(\omega-\omega'+\omega_0)+\delta(\omega-\omega'-\omega_0)]. \quad (44)$$

We assume that $\omega_0 = 0$, substitute (44) into (40), and let $T$ approach infinity:

$$\phi_2(\omega) = \frac{1}{\sin^2\theta}\frac{\sin^2\left(\pi\frac{\omega}{\omega_0}\right)}{\left(\pi\frac{\omega}{\omega_0}\right)^2}[\phi_D(\omega-\omega_0)+\phi_D(\omega+\omega_0)]. \quad (45)$$

We conclude from (37) and (45) that, knowing $\phi_D(\omega)$, it is then straightforward to find $\phi_1(\omega)$ and $\phi_2(\omega)$. We point out, however, that the assumption of isotropy implies that the variance of the Doppler velocity is independent of $\theta$ as well as $\omega_0$, whereas the power spectra $\phi_1(\omega)$ and $\phi_2(\omega)$ do not conserve variance. This can be seen by setting $\tau = 0$ in (27) and by inspection of (37) and (45).

According to (27) and (28), we can obtain $\phi_D(\omega)$ by specifying the longitudinal and transverse autocovariance functions $R_L(r)$ and $R_T(r)$. As mentioned above, this is based on the assumption that $r$ is small compared to the smallest external velocity length scale. Thus, only eddies in the locally isotropic region are important. However, in order to determine $\phi_D(\omega)$ we need to specify $R_L(r)$ and $R_T(r)$ for all displacements $r$, or the corresponding spectra

$$F_L(k) = \frac{1}{2\pi}\int_{-\infty}^{\infty} R_L(r)e^{-ikr}dr \quad (46)$$

and

$$F_T(k) = \frac{1}{2\pi}\int_{-\infty}^{\infty} R_T(r)e^{-ikr}dr \quad (47)$$

for all values of the wavenumbers $k$. Since the effect of larger eddies is assumed negligible, we make the approximation that the turbulence is fully isotropic for all wavenumbers and that there is only one independent external length scale. This means that $F_L(k)$ and $F_T(k)$ are related by (Lumley and Panofsky, 1964)

$$F_T(k) = \frac{1}{2}\left[F_L(k) - k\frac{dF_L}{dk}\right], -\infty < k < \infty. \quad (48)$$

We assume the following generalized form for the longitudinal velocity spectrum:

$$F_L(k) = \frac{ML_\mu^{5/3}}{[1+(L_\mu|k|)^2\mu]^{5/6}\mu}, \quad (49)$$

where $M$ (>0) is the inertial subrange multiplier with dimensions of length$^{4/3}$ × time$^{-2}$, and $\mu$ (>0) is a dimensionless constant. For large $|k|$, (49) becomes

$$F_L(k) = M|k|^{-5/3}. \quad (50)$$

Therefore, $M$ is given by (Lumley and Panofsky, 1964)

$$M = \frac{9}{55}\alpha\epsilon^{2/3}, \quad (51)$$

where $\alpha \approx 1.5$ is the Kolmogorov constant and $\epsilon$ is the rate of dissipation of turbulence kinetic energy.

The transition from high wavenumbers (the inertial subrange part of the spectrum where the turbulence is locally isotropic) to low wavenumbers is usually specified by $k_m$, which is the wave number at which the function $kF_L(k)$ has a maximum. The corresponding maximum wavelength is defined as

$$\lambda_m = 2\pi/k_m. \quad (52)$$

The length scale $L_\mu$ in (47) is then given by

$$L_\mu = \frac{\lambda_m}{2\pi}\left(\frac{3}{2}\right)^{1/2}\mu. \tag{53}$$

From (50) we see that the spectral behavior in the inertial subrange depends only on $M$. At smaller wavenumbers, however, the spectra depend also on $\mu$. We assume in our model that only the high wavenumber end of the spectrum (51) is of importance in determining $\phi_D(\omega)$, $\phi_1(\omega)$ and $\phi_2(\omega)$. We can verify this by keeping $M$ and $\lambda$ fixed, and observing the sensitivity of $\phi_D(\omega)$, $\phi_1(\omega)$ and $\phi_2(\omega)$ to changes in $\mu$. We note, however, that specification of $M$, $\lambda$ and $\mu$ precludes independent specification of the variance

$$\sigma_\mu{}^2 = \int_{-\infty}^{\infty} F_L(k)dk = \int_{-\infty}^{\infty} F_T(k)dk \tag{54}$$

and the integral length scale

$$l_\mu = \sigma_\mu{}^{-2}\int_0^\infty R_L(r)dr = \frac{\pi}{\sigma_\mu{}^2}F_L(0). \tag{55}$$

These quantities become

$$\sigma_\mu{}^2 = \frac{B\left(\frac{1}{2\mu},\frac{1}{3\mu}\right)}{\mu}\frac{\left(\frac{3}{2}\right)^{1/3}\mu}{(2\pi)^{2/3}}M\lambda_m{}^{2/3} \tag{56}$$

and

$$l_\mu = \frac{1}{2}\frac{\mu\times\left(\frac{3}{2}\right)^{1/2}\mu}{B\left(\frac{1}{2\mu},\frac{1}{3\mu}\right)}\lambda_m, \tag{57}$$

where

$$B(a,b) = \int_0^1 t^{a-1}(1-t)^{b-1}dt = \frac{\Gamma(a)\Gamma(b)}{\Gamma(a+b)} \tag{58}$$

is the complete beta function (Davis, 1965).

Using (48) and (49) we get

$$F_T(k) = \frac{4}{3}F_L(k) - \frac{5}{6}\frac{ML_\mu{}^{5/3}}{[1+(L_\mu|k|)^{2\mu}]^{5/6}\mu+1}. \tag{59}$$

We obtain the following analytical expressions for $R_L(r)$ and $R_T(r)$ for $\mu = \frac{1}{2}$ [which we call the Kaimal case (Kaimal et al., 1972)] and for $\mu = 1$ [the Kármán case (von Kármán, 1948)]. Lenschow and Stankov (1986) have found that $\mu$ in the convective atmospheric boundary layer seems to vary between these values.

For the Kaimal case:

$$F_L(k) = ML_{1/2}{}^{5/3}(1+L_{1/2}|k|)^{-5/3}, \tag{60}$$

$$F_T(k) = \frac{4}{3}F_L(k) - \frac{5}{6}ML_{1/2}{}^{5/3}(1+L_{1/2}|k|)^{-8/3}, \tag{61}$$

$$L_{1/2} = \frac{3}{4\pi}\lambda_m \approx 0.24\lambda_m, \tag{62}$$

$$l_{1/2} = \frac{1}{2}\frac{\frac{1}{2}\times\frac{3}{2}\times\Gamma\left(\frac{5}{3}\right)}{\Gamma(1)\times\Gamma\left(\frac{2}{3}\right)}\lambda_m = \lambda_m/4, \tag{63}$$

$$\sigma_{1/2}{}^2 = 3\left(\frac{3}{4\pi}\right)^{2/3}M\lambda_m{}^{2/3} \approx 1.15M\lambda_m{}^{2/3}, \tag{64}$$

$$R_L(r) = 3ML_{1/2}{}^{2/3}\left\{1-(r/L_{1/2})^{2/3} \times\left[\cos(r/L_{1/2})S\left(r/L_{1/2},\frac{1}{3}\right)-\sin(r/L_{1/2})C\left(r/L_{1/2},\frac{1}{3}\right)\right]\right\}, \tag{65}$$

$$R_T(r) = R_L(r) - ML_{1/2}{}^{2/3} \times\left\{\left[\cos(r/L_{1/2})-\frac{3}{2}\frac{r}{L_{1/2}}\sin(r/L_{1/2})\right]S\left(r/L_{1/2},\frac{1}{3}\right) -\left[\sin(r/L_{1/2})+\frac{3}{2}\frac{r}{L_{1/2}}\sin(r/L_{1/2})\right]C\left(r/L_{1/2},\frac{1}{3}\right)\right\}, \tag{66}$$

where

$$C(x,a) = \int_x^\infty t^{a-1}\cos t dt \tag{67}$$

and

$$S(x,a) = \int_x^\infty t^{a-1}\sin t dt \tag{68}$$

are incomplete gamma functions (Davis, 1965).

For the Kármán case:

$$F_L(k) = ML_1{}^{5/3}(1+(L_1k)^2)^{-5/6}, \tag{69}$$

$$F_T(k) = \frac{4}{3}F_L(k) - \frac{5}{6}ML_1{}^{5/3}(1+(L_1k)^2)^{-11/6}, \tag{70}$$

$$L_1 = \frac{(3/2)^{1/2}}{2\pi}\lambda_m \approx 0.20\lambda_m, \tag{71}$$

$$l_1 = \frac{1}{2}\frac{\left(\frac{3}{2}\right)^{1/2}\Gamma\left(\frac{5}{6}\right)}{\Gamma\left(\frac{1}{2}\right)\Gamma\left(\frac{1}{3}\right)}\lambda_m \approx 0.12\lambda_m, \tag{72}$$

$$\sigma_1{}^2 = \frac{\Gamma\left(\frac{1}{2}\right)\Gamma\left(\frac{1}{3}\right)}{\Gamma\left(\frac{5}{6}\right)}\frac{\left(\frac{3}{2}\right)^{1/3}}{(2\pi)^{2/3}}M\lambda_m{}^{2/3} \approx 1.41M\lambda_m{}^{2/3}, \tag{73}$$

$$R_L(r) = 2ML_1{}^{2/3}\frac{\sqrt{\pi}}{\Gamma(5/6)}\left(\frac{r}{2L_1}\right)^{2/3}K_{1/3}\left(\frac{r}{L_1}\right), \tag{74}$$

$$R_T(r) = R_L(r) - 2ML_1^{2/3}\frac{\sqrt{\pi}}{\Gamma(5/6)}\left(\frac{r}{2L_1}\right)^{4/3}K_{2/3}\left(\frac{r}{L_1}\right), \quad (75)$$

where $K_\nu(x)$ is the modified Bessel function of the second kind of order $\nu$ (Olver, 1965).

For convenience in presenting the results, we scale the variables as follows:

time:

$$T = \tau/(2r/U); \quad (76)$$

frequency:

$$\Omega = \omega/(U/2r), \quad (77a)$$

$$\Omega_0 = \omega_0/(U/2r); \quad (77b)$$

length:

$$\eta = r/\lambda_m, \quad (78a)$$

$$\zeta = \rho/\lambda_m = 2\eta[T^2 + \sin^2\theta \sin^2(\Omega_0 T/2)]^{1/2}; \quad (78b)$$

variance:

$$Q(\zeta) = R_L(\rho)/(M\lambda_m^{2/3}), \quad (79a)$$

$$\Delta Q(\zeta) = [R_T(\rho) - R_L(\rho)]/(M\lambda_m^{2/3}); \quad (79b)$$

$$r_D(T) = R_D(\tau)/(M\lambda_m^{2/3})$$
$$= Q(\zeta)(\sin^2\theta \cos\Omega_0 T + \cos^2\theta)$$
$$+ \Delta Q(\zeta)\sin^2\theta\left[\cos^2\left(\frac{\Omega_0 T}{2}\right) - \sin^2\left(\frac{\Omega_0 T}{2}\right)\times\frac{T^2 - \cos^2\theta}{T^2 + \sin^2\theta \sin^2\frac{\Omega_0 T}{2}}\right]; \quad (79c)$$

spectra:

$$\Psi_D(\Omega) = \frac{1}{M\lambda_m^{2/3}}\frac{U}{2r}\phi_D\left(\frac{U}{2T}\Omega\right), \quad (80a)$$

$$\Psi_1(\Omega) = \frac{1}{\cos^2\theta}\frac{\sin^2\left(\pi\frac{\Omega}{\Omega_0}\right)}{\left(\pi\frac{\Omega}{\Omega_0}\right)^2}\Psi_D(\Omega), \quad (80b)$$

$$\Psi_2(\Omega) = \frac{1}{\sin^2\theta}\frac{\sin^2\left(\pi\frac{\Omega}{\Omega_0}\right)}{\left(\pi\frac{\Omega}{\Omega_0}\right)^2}[\Psi_D(\Omega - \Omega_0) + \Psi_D(\Omega + \Omega_0)], \quad (80c)$$

$$\Psi_L(\Omega) = \frac{1}{M\lambda_m^{2/3}}\frac{1}{2r}F_L\left(\frac{\Omega}{2r}\right)$$
$$= \left(\frac{L_\mu}{\lambda_m}\right)^{5/3}\frac{1}{2\eta}\left\{1 + \left(\frac{L_\mu}{\lambda_m}\frac{|\Omega|}{2\eta}\right)^{2\mu}\right\}^{-5/6\mu}, \quad (80d)$$

$$\Psi_T(\Omega) = \left(\frac{L_\mu}{\lambda_m}\right)^{5/3}\frac{1}{2\eta}\left\{\frac{4}{3}\left(\frac{L_\mu}{\lambda_m}\frac{|\Omega|}{2\eta}\right)^{2\mu} + \frac{1}{2}\right\}\times\left\{1 + \left(\frac{L_\mu}{\lambda_m}\frac{|\Omega|}{2\eta}\right)^{2\mu}\right\}^{-5/6\mu - 1}. \quad (80e)$$

## 3. Results

In this section, we present and discuss computational results for both the Doppler velocity spectrum $\Psi_D(\Omega)$ and the transfer functions

$$H_L(\Omega) = \Psi_1(\Omega)/\Psi_L(\Omega) \quad (81)$$

and

$$H_T(\Omega) = \Psi_2(\Omega)/\Psi_T(\Omega) \quad (82)$$

for several values of the conical angle $\theta$, $\eta = r/\lambda_m$, and normalized rate of rotation $\Omega_0$. Since we have not been able to determine $\Psi_D(\Omega)$ analytically, we have calculated spectra using an 8192-point fast Fourier transform (FFT) algorithm. This rather large number of points insures a sufficient spectral resolution without spectral aliasing becoming a problem in the computed spectra. This does not imply that such a large number of points is required to resolve a measured velocity spectrum.

In principle, there are four free parameters in the expressions for $H_L(\Omega)$ and $H_T(\Omega)$: $\mu$, $\theta$, $\Omega_0$ (77b) and $\eta$ (78a). We use values of $\mu = \frac{1}{2}$ and 1. In order to determine reasonable ranges of values for $\theta$, $\Omega_0$ and $\eta$, we must first decide on a value for $r$. Our selection is based on a compromise between measuring far enough away from the aircraft fuselage that flow distortion is negligible, and not going out so far that the size of the measurement circle precludes resolving turbulence wavelengths that need to be measured. On the basis of these criteria, we select $r = 10$ m. A typical value for $\lambda_m$ in the convective boundary layer is 1000 m (Kaimal et al., 1976). Therefore, we have

$$\eta = 0.01. \quad (83)$$

Next, for the purpose of narrowing the range of parameter values, we crudely approximate the high frequency roll-off in the transfer functions (81) and (82) by the volume filtering of a cylinder with base of radius $a = r\sin\theta$ and height $h = 2\pi U/\omega_0$. There is no reason to have the rotation rate $\omega_0$ be so large that $h < a$ since the high frequency roll-off is determined by the largest linear dimension of the volume. Therefore, we set the upper limit for $\omega_0$ such that

$$h > a, \quad (84)$$

or equivalently,

$$\Omega_0 < \frac{4\pi}{\sin\theta} \sim 20 \quad (85)$$

provided $\theta$ is not too small. A typical true airspeed for aircraft is $U = 100$ m s$^{-1}$. Thus, the upper limit for the rate of revolution is

$$f_0 = \frac{\omega_0}{2\pi} < \frac{U}{r \sin\theta} \sim 20 \text{ Hz}. \quad (86)$$

This upper limit seems just outside technical feasibility.

We carried out computations for $\Omega_0 = 0.5$, 1, 2, 4, 8, 16 and 32 (corresponding to $f_0 \approx 0.4$, 0.8, 1.6, 3.2, 6.4, 13 and 25 Hz), and for $\theta = 30°$, 45° and 60°. First, $\Psi_D(\Omega)$ was computed using the FFT. In order to calculate $\Psi_D(\Omega - \Omega_0) + \Psi_D(\Omega + \Omega_0)$ we must first take into account that the spectrum calculated in this way is periodic in $\Omega$ with the period twice the Nyquist frequency $\Omega_N$; i.e.,

$$\Psi_D(\Omega + 2m\Omega_N) = \Psi_D(\Omega), \quad m \text{ an integer}. \quad (87)$$

Further, the method only provides spectral estimates in the range $0 < \Omega \leq \Omega_0$. However, since

$$\Psi_D(-\Omega) = \Psi_D(\Omega) \quad (88)$$

we have, for $0 < \Omega \leq \Omega_0$, the identity

$$\Psi_D(\Omega - \Omega_0) = \Psi_D(\Omega - \Omega_0 + 2\Omega_N). \quad (89)$$

The power spectrum of the Doppler velocity $\Psi_D(\Omega)$ as well as the spectral transfer functions $H_L(\Omega)$ and $H_T(\Omega)$, are plotted in Fig. 3 for $\theta = 45°$, $\Omega_0 = 1$ and $\eta = 0.01$. We note, not surprisingly, that a resonance occurs in $\Psi_D(\Omega)$ at the normalized frequency $\Omega_0$. Furthermore, there is a single peak at $\Omega_0$ for the Kaimal case ($\mu = \frac{1}{2}$) and a double peak for the Kármán case ($\mu = 1$). We have no explanation for this peculiarity.

We also plot the transfer functions $H_L(\Omega)$ and $H_T(\Omega)$ in Fig. 4 for four cases: $\Omega_0 = 1$ and $\theta = 30°$ and 60°; and $\theta = 45°$ and $\Omega_0 = 0.5$ and 2. We note that the transfer functions do not, in general, seem to approach unity as $\Omega \to 0$. This seems to contradict the discussion in connection with (6)–(8) that, for wind fields that vary slowly in space and time, the measurement technique provides the correct velocity components. However, for the cases presented here, the conical scan rate is not fast enough compared to the time scale of the velocity fluctuations to give unity transfer functions as $\Omega \to 0$; that is, the condition that $\omega_0 \gg (2\pi/\lambda_m)U$ or equivalently, $2\pi\eta \ll \Omega_0/2$ is not fulfilled. We have found that for $\theta \approx 45°$, $\Omega_0 > 1$ results in transfer functions within a few percent of unity as $\Omega \to 0$. Figure 5 shows an example of a nearly unity transfer function as $\Omega \to 0$ with $\theta = 45°$ and $\Omega_0 = 4$.

The transfer functions go to zero at $\Omega = \Omega_0$. Although we do not show the transfer functions for $\Omega_0 > 4$, we can see in Fig. 5 that the transfer functions are already significantly modified at $\Omega/\Omega_0 = 0.25$, while, as shown in Fig. 4, for $\Omega_0 = 0.5$, 1 and 2, the high-frequency cutoff for the longitudinal transfer functions is sharper. The results for $\Omega_0 = 8$ (not shown) are somewhat better than for $\Omega_0 = 4$, although the high-frequency cutoff for the longitudinal transfer functions becomes flatter. On the basis of these results, we conclude that with $\Omega_0 = 4$, the longitudinal and transverse velocity components

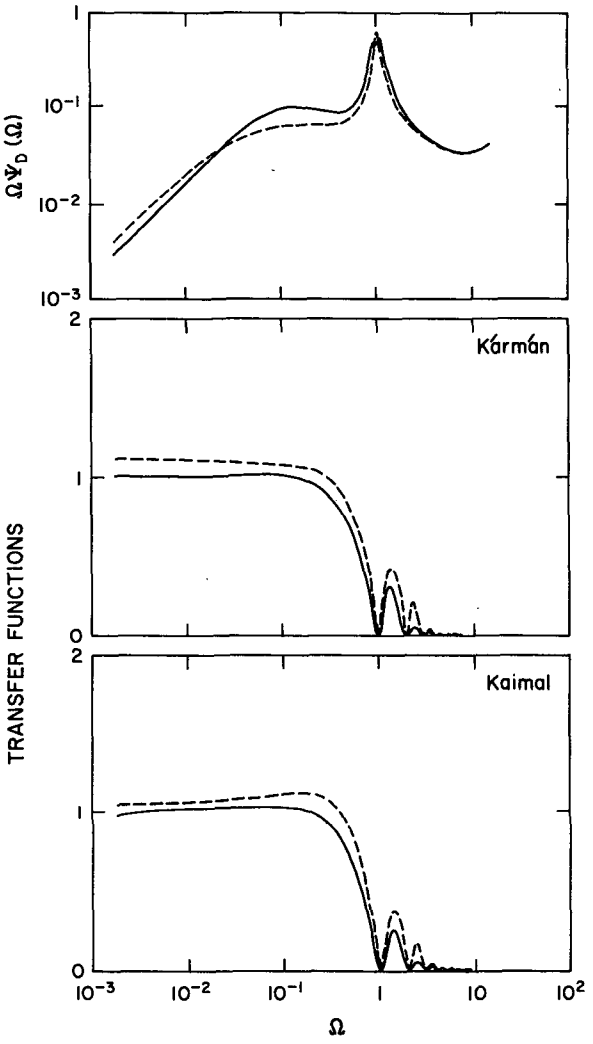


FIG. 3. Power spectra of the Doppler velocity multiplied by normalized frequency $\Omega\Psi_D(\Omega)$ and transfer functions $H_L(\Omega)$ and $H_T(\Omega)$ for $\theta = 45°$, $\Omega_0 = 1$ and $\eta = 0.01$. The solid line in top panel is the von Kármán case and the dashed line is the Kaimal case. The solid lines in the other panels are longitudinal transfer functions and the dashed lines transversal transfer functions.

can be measured without correction up to $\Omega \sim 0.5$. Furthermore, it seems likely that, in practice, the spectra can be corrected up to $\Omega \sim 3$. For $\Omega_0 > 4$, some improvement is still possible, but the frequency limit can probably not be extended by more than about a factor of 2.

Using (77a) and Taylor's hypothesis means that, for $\Omega_0 = 4$, and an aircraft speed of 100 m s$^{-1}$, we can measure spectra without correction up to $k \approx 0.025$ rad m$^{-1}$ or $\lambda \approx 250$ m, and with corrections $k \approx 0.15$ rad m$^{-1}$ or $\lambda \approx 40$ m. Since $\lambda_m$ is typically of order 1000 m in the convective boundary layer, this means that velocity spectra can be measured well into the in-

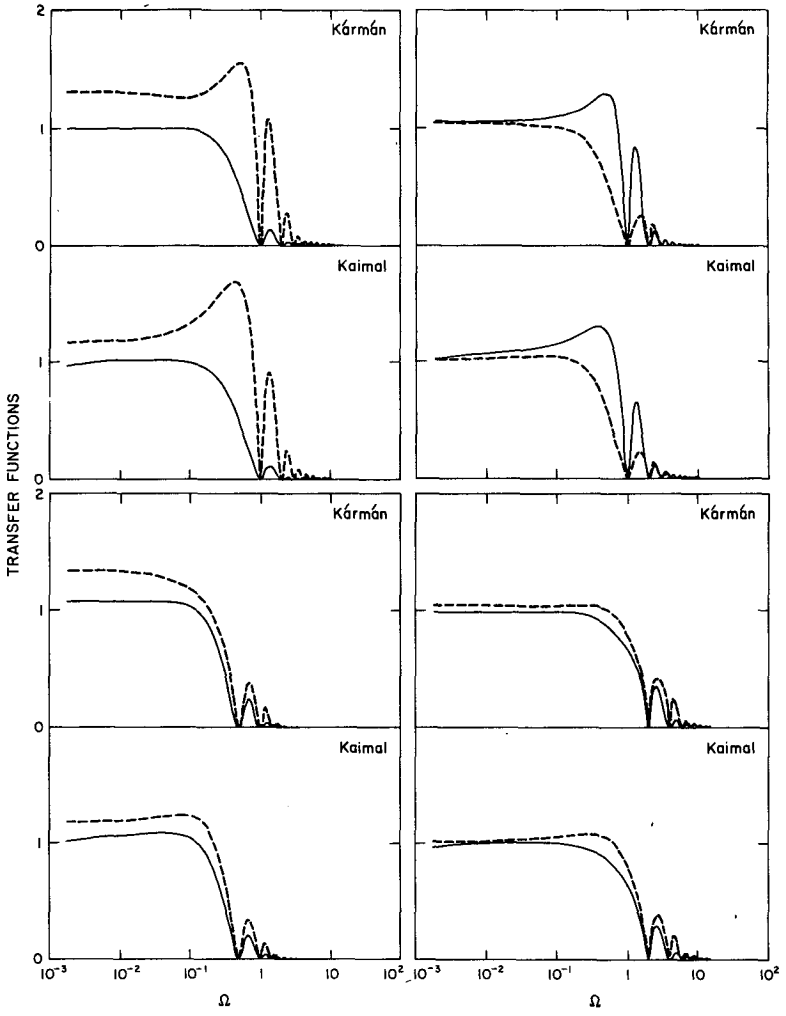


FIG. 4. Transfer functions $H_L(\Omega)$ and $H_T(\Omega)$ for $\eta = 0.01$. Top left: $\theta = 30°$ and $\Omega_0 = 1$; top right: $\theta = 60°$ and $\Omega_0 = 1$; bottom left: $\theta = 45°$ and $\Omega_0 = 0.5$; bottom right: $\theta = 45°$ and $\Omega_0 = 2$. The solid lines are longitudinal and dashed lines transversal transfer functions.

ertial subrange. As discussed by Keeler et al. (1986) the expected measurement uncertainty is likely to be considerably less than the actual velocity fluctuations in the boundary layer, and therefore, measurement uncertainties need not be considered in this analysis.

This does not mean that the individual eddies themselves can be accurately resolved along the longitudinal axis of the aircraft by using the transfer function to correct for the amplitude reduction, since the velocity estimates are obtained along a helical trajectory around the longitudinal axis of the aircraft. We conservatively estimate that the individual eddies can be resolved with negligible distortion up to at least $\Omega \approx 1$, or $k \approx 0.05$ rad $m^{-1}$ and $\lambda \approx 120$ m. Above this frequency, the transfer functions begin to decrease rapidly. This means that velocity covariances, as well as covariances of velocity components and scalars (e.g., temperature and trace constituent concentrations) measured on the longitudinal axis of the aircraft can be resolved up to at least $\Omega \approx 1$, but probably not much greater than this.

## 4. Mean wind shear

The lidar scanning technique proposed here measures the Doppler velocity over a circle whose radius is large enough that mean shear can create significant differences in the measured wind components across the circle. Some examples of situations where these differences may be significant include flight legs in the capping inversion of a convective boundary layer, in the nocturnal boundary layer, and in fronts, orographically forced flows, downbursts and other mesoscale phenomena.

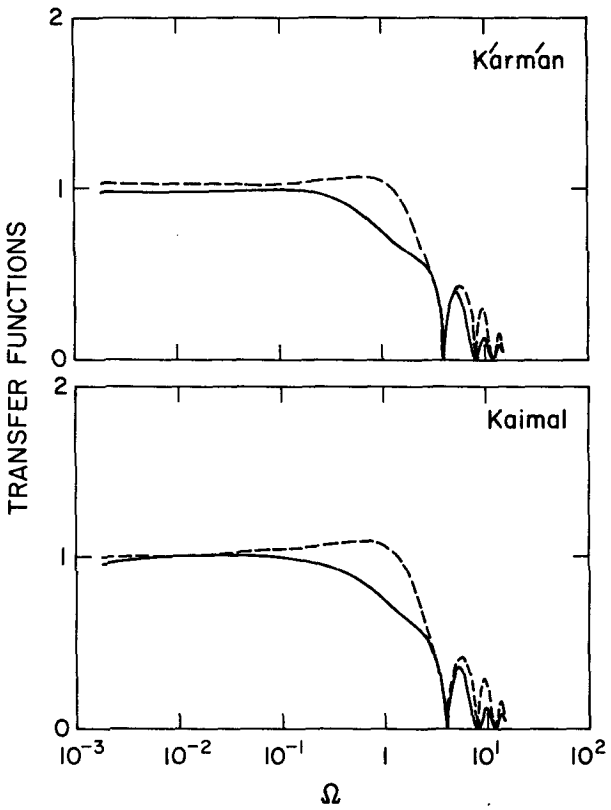


FIG. 5. Transfer functions $H_L(\Omega)$ and $H_T(\Omega)$ for $\theta = 45°$, $\Omega_0 = 4$ and $\eta = 0.01$. The solid lines are longitudinal and dashed lines transversal transfer functions.

We investigate the effects of mean wind shear on the measured wind components by first writing an expression for the measured mean wind field with a constant shear $A_{ij} = \langle \partial u_i/\partial x_j \rangle$ evaluated at the point $r_i = -r\cos\theta\delta_{1i}$. For mathematical convenience, we use tensor notation (with summation denoted by repeated indices). The mean wind field is

$$[u_i(\mathbf{r}, t)] = U_i + A_{ij}(r_j + r\cos\theta\delta_{1j}), \tag{90}$$

where $U_i$ is the constant mean wind and $\delta_{ij}$ is the Kronecker delta. We assume horizontal homogeneity, so that

$$A_{ij} = A_{13}\delta_{1i}\delta_{3j} + A_{23}\delta_{2i}\delta_{3j}. \tag{91}$$

As before, we measure along the circle

$$r_i(t) = -r\cos\theta\delta_{1i} + r\sin\theta\cos(\omega_0 t)\delta_{2i} + r\sin\theta\sin(\omega_0 t)\delta_{3i}. \tag{92}$$

The measured mean Doppler velocity then becomes

$$\langle u_D(t)\rangle = \langle u_i[\mathbf{r}(t), t]\rangle \frac{r_i(t)}{r}$$
$$= -U_i\cos\theta + (-rA_{13}\cos\theta + U_3)\sin\theta\sin\omega_0 t$$
$$+ (U_2 + rA_{23}\sin\theta\sin\omega_0 t)\sin\theta\cos\omega_0 t. \tag{93}$$

Substituting (93) into (6), (7) and (8), we find that only the $x_1$-component of the wind shear, i.e., $A_{13}$ affects the mean wind velocity, and only the $U_3$-component is affected. We have

$$U_3 = \frac{\omega_0}{\pi\sin\theta}\left\langle \int_{t-2\pi/\omega_0}^{t} u_D(t')\sin\omega_0 t'dt' \right\rangle - A_{13}r\cos\theta. \tag{94}$$

For a wind shear of $A_{13} = 0.01\ \text{s}^{-1}$, this term adds an error to $U_3$ of $0.07\ \text{m s}^{-1}$ at a scanning angle of $\theta = 45°$. Since Keeler et al. (1986) estimate that the velocity measurement uncertainty is about $\pm 0.02\ \text{m s}^{-1}$ for an integration time of 2.5 ms, in certain situations, the shear may add a significant error to the estimate of vertical velocity.

One way that this term can be estimated is by varying the scanning angle $\theta$. Another, perhaps somewhat simpler, possibility is to use a second lidar beam pointing vertically. In this way, $U_3$ can be measured directly and $A_{13}$ can then be obtained from (94). In addition to its use for estimating the $x$-component of shear, a redundant measurement of $u_3$ could be very useful since $u_3$ is usually smaller in magnitude than the other two wind components, particularly at low frequencies. Furthermore, the redundant $u_3$ measurement might be more useful for flux calculations than the scanning estimate since the measurement might be closer to the location of the other sensors, and could be sampled more frequently.

Although the $y$-component of shear does not contribute to the velocity components obtained from (6)–(8), it can be estimated from the expression

$$A_{23} = \frac{4\omega_0}{\pi r\sin^2\theta}\left\langle \int_{t-2\pi/\omega_0}^{t} u_D(t')\cos\omega_0 t'\sin\omega_0 t'dt' \right\rangle. \tag{95}$$

Thus no additional measurements are required to obtain the $y$-component of shear—only an additional computation.

Wind shear measurements by the lidar scanning technique have the potential for opening up new areas of airborne research. Wind shear is the forcing function for turbulence in stably stratified regions of the atmosphere, and thus is directly related to entrainment processes at the top of the convective boundary layer, generation of clear-air turbulence, and turbulence and diffusion in the nocturnal boundary layer. By combining wind shear with vertical temperature gradient measurements from either a scanning infrared radiometer or two vertically displaced thermometers, it should be possible to estimate the gradient Richardson number while simultaneously measuring turbulence quantities such as variances and fluxes on constant-level flight legs.

## 5. Concluding remarks

We have shown that for locally isotropic turbulence, assuming Taylor's hypothesis is fulfilled, it is theoret-

ically possible to measure power spectra of the longitudinal and transverse velocity components from an aircraft with the conically scanning technique. The analysis shows that the spectra can be measured without significant correction out to $r/\lambda \sim 0.04$, and with correction to $r/\lambda \sim 0.25$, at a scanning rate of $\sim$3.2 Hz for typical aircraft speeds, and that at least 80% of the total contribution to vertical fluxes of scalar variables can be resolved by aircraft measurements in the convective boundary layer.

The assumptions that we have made in this analysis seem to be realistic for a convective atmospheric boundary layer. Therefore, we believe that the next step is to carry out further experiments in the boundary layer to make sure that there are no unanticipated technical or conceptual difficulties with this approach. The initial results reported by Keeler et al. (1986) are encouraging. If further experimental work verifies our theoretical model, we suggest that further refinement of the theoretical model is justified. One suggestion is to include the effects of volume averaging that is inherent in using a continuous-wave optically focused beam.

On the basis of the results presented here, we believe that the technique offers many advantages over presently used in situ sensors for measuring air motion from an aircraft, and offers a potential new capability for measuring wind shear.

*Acknowledgments.* We wish to express our gratitude to Ron Schwiesow, Bob Serafin and Jeff Keeler for initiating and encouraging the concept of a conically scanning airborne Doppler lidar. Peter Kirkegaard of Risø National Laboratory, Denmark deserves thanks for help in setting up the computer programs, and Hope Hamilton and Janell Petersen for the painstaking job of typing the manuscript with all its complicated equations.

## REFERENCES

Caughey, S. J., and J. C. Kaimal, 1977: Vertical heat flux in the convective boundary layer. *Quart. J. Roy. Meteor. Soc.*, **103**, 811–815.

Davis, P. J., 1965: Gamma function and related functions. *Handbook of Mathematical Functions.* M. A. Abramowitz and I. A. Stegun, Eds., Dover, 253–293.

Kaimal, J. C., J. C. Wyngaard, Y. Izumi and O. R. Cote, 1972: Spectral characteristics of surface layer turbulence. *Quart. J. Roy. Meteor. Soc.*, **98**, 563–589.

——, ——, D. A. Haugen, Y. Izumi, S. J. Caughey and C. J. Readings, 1976: Turbulence structure in the convective boundary layer. *J. Atmos. Sci.*, **33**, 2152–2169.

Keeler, R. J., R. J. Serafin, R. L. Schwiesow, D. H. Lenschow, J. M. Vaughan and A. Woodfield, 1986: An airborne laser air motion sensing system. Part I: Concept and preliminary experiment. *J. Atmos. Oceanic Technol.*, In press.

Lenschow, D. H., 1986: Aircraft measurements in the boundary layer. *Probing the Atmospheric Boundary Layer,* D. H. Lenschow, Ed., Amer. Meteor. Soc., 39–55.

——, and B. B. Stankov, 1986: Length scales in the convective atmospheric boundary layer. *J. Atmos. Sci.*, in press.

Lumley, J. L., and H. A. Panofsky, 1964: *The Structure of Atmospheric Turbulence.* Interscience Monographs and Texts in Physics and Astronomy, Wiley and Sons, 239 pp.

Olver, F. W. J., 1965: Bessel functions of integer order. *Handbook of Mathematical Functions,* M. Abramowitz and I. A. Stegun, Eds., Dover, 355–433.

von Kármán, T., 1948: Progress in the statistical theory of turbulence. *Proc. Natl. Acad. Sci. (U.S.),* **34**, 530–539.